Bulletin of the Seismological Society of America, Vol. 93, No. 2, pp. 804–816, April 2003

T-Wave Detection of Two Underwater Explosions off Hawaii on 13 April 2000

by Dominique Reymond, Olivier Hyvernaud, Jacques Talandier, and Emile A. Okal

Abstract We studied two presumed underwater explosions, detonated on 13 April 2000 (approximate times 00:19 and 23:29 coordinated universal time), at a site located approximately 215 km southwest of Oahu, Hawaii, and detected from a combination of *T* phases recorded at shore-based seismic stations and acoustic waves recorded by hydrophones. The explosions were initially detected by the Polynesian Seismic Network, and a preliminary location obtained in the vicinity of Kauai. With the use of an enlarged dataset, an improved location was obtained, after correcting arrival times for both the influence of the seismic path at the receivers, and the effect of dispersion along the acoustic path. The explosive nature of the source was tested using several criteria: the duration–amplitude discriminant of Talandier and Okal (2001), the variation of spectral amplitude with frequency, the observation of a strong frequency dispersion in the spectrograms, and the identification of a bubble period (0.45 sec) in the cepstra of the signals, which translates into a yield of 275 kg of equivalent TNT for a depth of 50 m. In the context of monitoring the Comprehensive Nuclear Test Ban Treaty, these two explosions provide a perfect opportunity to assess the capabilities of *T*-phase stations and hydrophones for detection, location, identification, and quantification of these sources. Our study, conducted in the absence of any ground-truth information, stresses the possibility of a powerful synergy between these two types of recording facilities, but also points to several limitations in the performance of certain shore-based seismic stations.

Introduction

This article studies two presumed underwater explosions, detonated on 13 April 2000, approximately 215 km southwest of Oahu, Hawaii, and detected from a combination of *T* phases at shore-based seismic stations and acoustic waves recorded by hydrophones. In the context of monitoring the Comprehensive Nuclear Test Ban Treaty (CTBT), these sources provide a perfect opportunity to assess the capabilities of *T*-phase stations and hydrophones for detection, location, identification, and quantification of marine events. They illustrate the power of synergy between the two types of recording facilities, but also point to limitations in the performance of certain shore-based seismic stations.

The two explosions, hereafter events I and II, were detected during routine seismic processing at the Central Laboratory of the Polynesian Seismic Network (hereafter, RSP) in Papeete, Tahiti, on Thursday, 13 April 2000 local time (event I) and Friday, 14 April 2000 (event II). This network has been described in previous publications (Talandier and Kuster, 1976; Okal *et al.*, 1980); it includes short-period stations equipped with special band-pass filters in the frequency range 2–10 Hz. Such instrumentation, initially developed in the 1970s, has helped define the concept of so-called "*T*-phase stations," later mandated by the CTBT (Okal, 2001).

In the absence of Station RKT (Gambier Islands), temporarily shut down for maintenance and upgrade during the Spring of 2000, records were obtained from three main sites in Polynesia: PMO in the Tuamotu Islands, PPT in the Society Islands, and TBI in the Austral Islands. This regional dataset provided minimal azimuthal coverage (<6°), and resulted in only a very crude epicentral estimate (11° N, 157° W) with essentially no constraint on distance. Thus, a systematic effort to gather as many records as possible from other Pacific sites was carried out during the following weeks and months, as continuous data became available. As detailed in Table 1, records were obtained from IRIS and PIDC stations, the Canadian National Seismic Network (CNSN), the Eastern Equatorial Pacific Autonomous Hydrophone Array (Fox *et al.*, 2001), the broadband station operated at Honolulu Observatory (HON) by the Pacific Tsunami Warning Center, and Station KAA on the west coast of the Island of Hawaii, operated by the Hawaiian Volcano Observatory. A number of sites were further explored in the hope of obtaining additional records, but unsuccessfully, for

Table 1
Seismic and Acoustic Stations Used in This Study

Code	Name	Island	Archipelago	Network	Coordinates (°N)	Coordinates (°E)	Sampling Rate (Hz)	Epicentral Distance to Event I (km)
PMO	Pomariorio	Rangiroa	Tuamotu	RSP	−15.017	−147.906	50	4073
PPT	Papeete	Tahiti	Society	RSP	−17.569	−149.574	50	4293
TBI	Tubuai	Tubuai	Austral	RSP	−23.349	−149.461	50	4916
XMAS	Kiritimati	Christmas	Line	IRIS	2.045	−157.445	20	1996
KIP	Kipapa	Oahu	Hawaii	IRIS	21.420	−158.020	20	225
HON	Honolulu	Oahu	Hawaii	PTWC	21.322	−158.008	100	219
KAA	Kaapuna	Hawaii	Hawaii	HVO	19.266	−155.871	100	392
BNB	Barry Inlet			CNSN	52.576	−131.752	100	4339
WK30	Wake Hydrophone			IDC	19.410	165.856	240	3623
WK31	Wake Hydrophone			IDC	17.927	167.499	240	3474
H25	East Pac. Hydrophone			EEPHA	−7.992	−109.937	250	6251
No signal above noise level								
KWAJ	Kwajalein	Kwajalein	Marshall	IRIS				
OGS	Ogasawara	Chichi-jima	Bonin	POSEIDON				
PTCN	Pitcairn	Pitcairn	Pitcairn-Gambier	IRIS				
WAKE	Wake Island	Wake		IRIS				
RPN	Rapa Nui	Easter		IRIS				
BNB	Barry Inlet			PIDC	Event II only			
No data available								
AFI	Afiamalu	Upolu	Samoa	IRIS				
JOHN	Johnston	Johnston		IRIS				
KIP	Kipapa	Oahu	Hawaii	IRIS	Event II only			
MIDW	Midway	Sand	Hawaii-Emperor	IRIS				
RAR	Rarotonga	Rarotonga	Cook	IRIS				
RKT	Rikitea	Mangareva	Pitcairn-Gambier	RSP				

a variety of reasons discussed in the Discussion and Conclusions section.

Our analysis focuses primarily on event I, and the very similar results obtained for event II are simply mentioned for reference. Figure 1 shows a general map of the stations used in this study.

We wish to emphasize that our results are presented here without the benefit of any ground-truth information. We report the events as explosions, but to the best of our knowledge at the time of writing (10 October 2002), these sources have not been announced. Our estimates of epicentral coordinates, origin times, and tentative values of yield are published in the hope that they may be compared with ground-truth data, if and when the latter become available in the future, thus providing further insight into the detection capabilities and performance of *T*-phase and hydroacoustic stations.

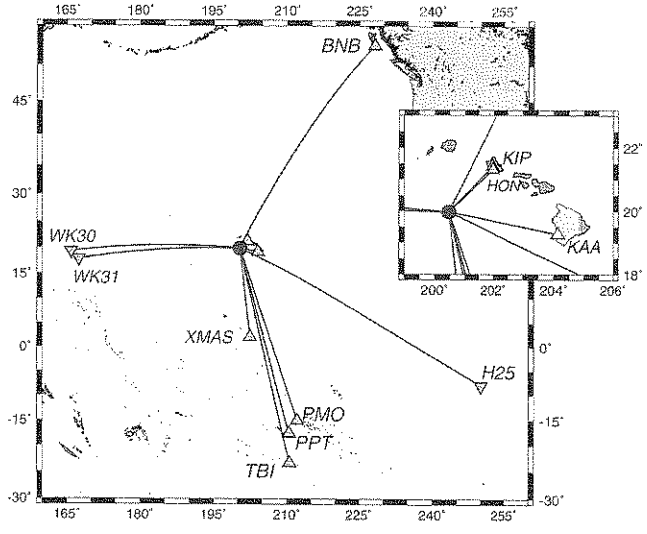

Figure 1. Map of the epicenter of event I (solid dot) and of the stations used in this study (seismic, upward triangles; hydrophones, inverted triangles). The inset details the position of the shot with respect to the Hawaiian Islands. Note that the paths to BNB and H25 are unobstructed by the islands. Even on the scale of the inset, event II would not be distinguishable from event I.

Data Processing and Source Location

All records were systematically processed using a standardized algorithm illustrated in Figure 2. A 20.47-s time series containing the *T* phase was first extracted, high-pass filtered ($f \geq 2$ Hz), and plotted in the lower box. This record was used to measure the envelope of ground velocity (e_{Max}),

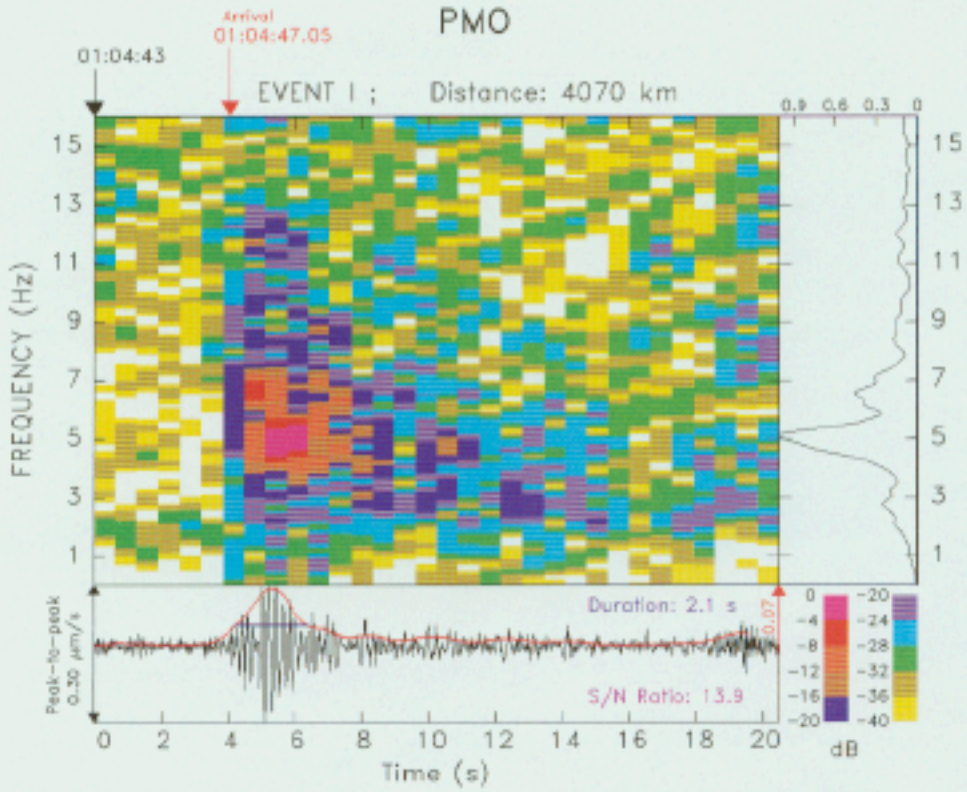

Figure 2. Example of standardized processing of a *T*-phase record. The figure is composed of three frames. The bottom frame shows a 20.47-sec window of the original time series of the ground velocity (in black), high-passed filtered for $f \geq 2$ Hz. The red curve is the envelope of the signal computed following the algorithm of Talandier and Okal (2001); the red arrow and scale at right (in micrometers per second) are used for the computation of the parameter e_{Max}. The blue line across the main wavepacket illustrates the computation of its duration, $\tau_{1/3}$ (Talandier and Okal, 2001), which is printed in the upper-right-hand corner of the frame. An estimate of the signal-to-noise ratio is also given. The frame at right is a plot of the amplitude spectrum of the high-pass filtered ground velocity record. The main color frame is a spectrogram representation of the distribution of spectral amplitude in the record, as a function of time and frequency. The color coding is logarithmic, with the key (in decibels relative to the most energetic pixel) given at bottom right. White pixels correspond to spectral amplitudes below −40 dB.

and the duration of the phase ($\tau_{1/3}$), as described by Talandier and Okal (2001). The record was then Fourier-transformed, and the resulting spectral amplitude plotted vertically in the upper-right-hand side box, using a linear scale. The main diagram on Figure 2 is a spectrogram illustrating the level of spectral amplitude carried by the *T* phase as a function of time and frequency; the sampling on the spectrogram is 0.64 sec in time and 0.05 Hz in frequency. The palette on Figure 2 is logarithmic with a step of 4 dB with respect to the pixel with maximum amplitude in each seismogram.

Determination of Arrival Time

A first estimate of the arrival time at each station was obtained by picking the onset of arrival. In the example of Figure 2, this time corresponds to a sudden increase of more than 20 dB in the level of spectral amplitude. The set of these 11 uncorrected travel times was then used to obtain a first-order solution, by inverting for epicentral location and origin time, using the laterally heterogeneous velocity model of Levitus *et al.* (1994), gridded at a sampling of 1°, and seasonally averaged. The source locates at 19.997° N, 159.527° W, with an origin time of 00:19:00.4 coordinated universal time. The standard deviation of the residual travel times is $\sigma = 2.24$ sec. This epicenter is shown as the upward-pointing triangle on the left-hand side of Figure 3.

Travel-Time Corrections

The previously mentioned solution was then refined through the introduction of two sets of travel-time corrections.

Seismic Path Correction C. With the obvious exception of the hydrophone records from WK30, WK31, and H25, we applied a correction, *C*, taking into account the propagation

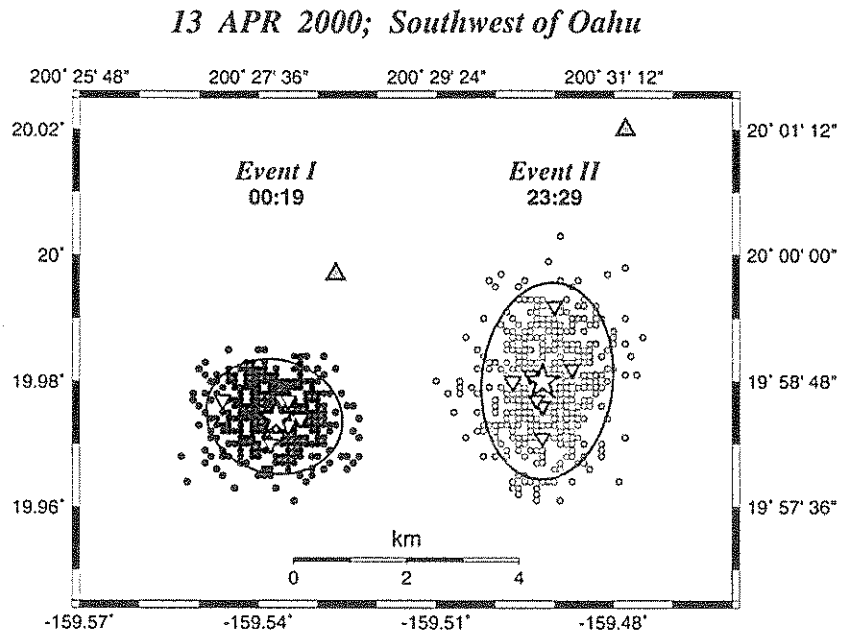

Figure 3. Detailed location of the epicenters of the two events. The best locations, obtained from the full, corrected, datasets, are given as the open stars. The cluster of dots (solid for event I; open for event II) are the Monte Carlo epicenters with $\sigma_G = 1.5$ sec. The jackknifed solutions are shown as inverted triangles; in event I, the larger, open symbol relates to the elimination of H25. Finally, the upward-pointing triangles show epicenters relocated without the corrections C and C_D.

of the T phase as a seismic wave following conversion at the receiving shore, as detailed by Talandier and Okal (1998). For stations PMO and XMAS, located on atolls, in the immediate vicinity of the shoreline, C is negligible.

This correction, which is added to the measured arrival time to mimic full propagation as an acoustic wave in the water, is always positive.

Frequency Dispersion Correction C_D. This second correction is motivated by the fact that waves guided by the SOFAR channel are inversely dispersed, and that seismic records of T phases are of significantly lower frequency than the waves typically used in the determination of acoustic velocity models such as the model of Levitus *et al.* (1994). We use the following expression for the group velocity dispersion of T waves generated by marine explosions in the Pacific Ocean.

$$V(f) = 1483.3 - \frac{4.7}{f - 0.5} \qquad (1)$$

where the velocity $V(f)$ is in meters per second and the frequency f is in hertz. This formula was derived empirically from records in Polynesia of a series of controlled-source experiments with published epicenters and origin times (Nava *et al.*, 1988; Taber and Lewis, 1986; B. T. R. Lewis, personal comm., 2000).

We then compute the correction C_D by evaluating the dominant frequency f_0 of the wave packet retained as first arrival, and adjusting the travel time to a velocity $V_L = 1483.0$ m/s, representative of the average speed derived from the models of Levitus *et al.* (1994) in the geographic region involved:

$$C_D = d \cdot \left[\frac{1}{V_L} - \frac{1}{V(f_0)}\right] \qquad (2)$$

The correction C_D, which is always negative, is added to the arrival time. In this formula, d is the epicentral distance, in kilometers, for the uncorrected epicenter. In practice, we find it unnecessary to correct the hydrophone records (at WK30, WK31, and H25) whose dominant frequencies in the first wave packets are approximately 12 Hz, and the Hawaiian stations (KIP, HON, and KAA), for which distances are short, and hence $|C_D|$ is less than 0.2 sec.

The corrected travel times are then used to refine the source parameters. The inversion quickly converges to an epicenter at 19.974° N, 159.537° W, with an origin time of 00:19:01.0 coordinated universal time. This location is shown as a large star on Figure 3. The standard deviation σ of the residuals is only 1.38 sec, with only station H25 featuring a large residual (-3.51 sec).

Monte Carlo Relocations

The precision of the solution is investigated first through a Monte Carlo algorithm (Wysession *et al.*, 1991), which consists of carrying out a large number of relocations after injecting Gaussian noise with standard deviation σ_G into the dataset. Here we take $\sigma_G = 1.5$ sec, a value greater than the standard deviation σ of the residuals, and iterate the process 500 times. The results are shown as the solid dots on Figure 3. Note that the solution is remarkably robust, with the best-fitting ellipse covering only about 5 km^2.

Jackknifing

The quality of the solution was further investigated by "jackknifing" the dataset, which consists of systematically suppressing one datum at a time (Thomson and Chave, 1991). This procedure provides an alternative means of estimating the robustness of the solution, and in particular, of identifying the importance of each element of the dataset.

The resulting epicenters are plotted as inverted triangles on Figure 3, the solution without H25 using a larger, open symbol. It is immediately apparent that jackknifed epicenters are displaced less than 0.5 km from the full solution, except in the case of H25 (1 km). Furthermore, all jackknifed epicenters, including the latter one (with H25 suppressed), fall within the Monte Carlo ellipse for the full solution, which emphasizes the robust nature of the solution.

Event II

In the case of event II, no signals are available at KIP after 21:43 coordinated universal time. In addition, the records at PPT and BNB could not be processed, the signals failing to satisfactorily emerge from background noise. Relocation using corrected travel times at the eight available stations yields an epicenter at 19.980° N, 159.492° W, with an origin time of 23:29:13.7 coordinated universal time. As expected from the smaller dataset, Figure 3 shows that the Monte Carlo ellipse for the same Gaussian noise ($\sigma_G = 1.5$ sec) is substantially larger than for event I, but still includes all jackknifed epicenters. On the other hand, the two preferred epicenters are separated by 4.75 km, and their Monte Carlo ellipses do not intersect, suggesting that the two events have distinct epicenters.

Identification of the Nature of the Sources: the Duration–Amplitude Discriminant

In this section, we apply the discriminant introduced by Talandier and Okal (2001), and identify events I and II as underwater explosions. These authors showed that the parameter

$$D = \log_{10} e_{\mathrm{Max}} - 4.9 \log_{10} \tau_{1/3} + 4.1 \qquad (3)$$

effectively separates underwater explosive sources (for which $D > 0$) from most earthquake sources ($D < 0$) in the oceanic environment. In equation (3), e_{Max} is the amplitude (in micrometers per second) of the envelope of the ground velocity signal recorded at a *T*-wave station, and $\tau_{1/3}$ the time (in seconds) during which the envelope signal keeps a sustained amplitude of at least one third its maximum, measured above the background noise level. Talandier and Okal (2001) showed that the performance of D is optimized at atoll stations; in the present context, this restricts the method to XMAS and PMO, where we obtained D-values of 1.46 and 2.12, respectively, for event I, and 0.59 and 2.37 for event II. As shown on Figure 4, the discriminant clearly identifies both events at both stations as underwater explosions.

Shape of Spectrum as a Function of Frequency and Bubble Effects

We study here the shape of the amplitude spectra of the T-phase records of events I and II, and their variation with frequency, which we find oscillatory; we further identify a

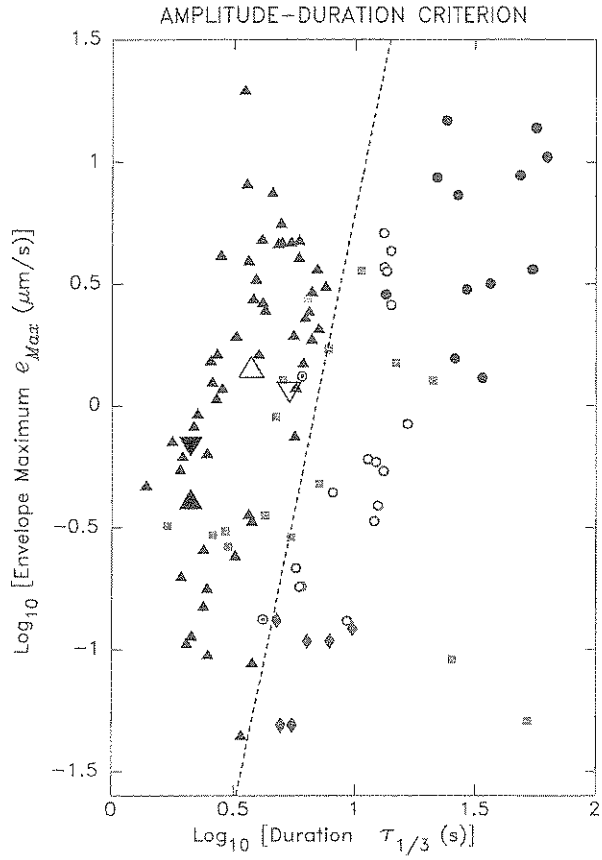

Figure 4. This figure is adapted from figure 6 of Talandier and Okal (2001) and applies their amplitude–duration discriminant to the Hawaiian events of 13 April 2001. The discriminant (3) vanishes along the dashed line, separating explosions (above and to the left) from earthquakes (below and to the right). See Talandier and Okal (2001) for a full description of the individual smaller symbols. The large triangles relate to records of events I (upward pointing) and II (downward pointing) at PMO (solid symbols) and XMAS (open symbols), respectively. They clearly characterize the two events as underwater explosions.

"bubble" spike in their cepstra, leading to a tentative quantification of the sources. These results strongly support the interpretation of the events as underwater explosions.

We are motivated by our empirical observation that a large number of T-phase records from earthquakes and explosions can be discriminated on the basis of the variation with frequency of the spectral amplitude of ground velocity, $X(f)$. This is illustrated on Figure 5a in the case of a teleseismic earthquake near the Alaska Peninsula (14 March 1995; $m_b = 6.1$), and an explosion south of Vancouver Island (21 August 1980), recorded on Polynesian atoll stations at comparable maximum spectral amplitudes for their *T* phases. It is clear that the earthquake spectrum decays both quickly and smoothly with frequency, whereas the explosion spectrum decays slowly, if at all, and exhibits large variations about its mean trend.

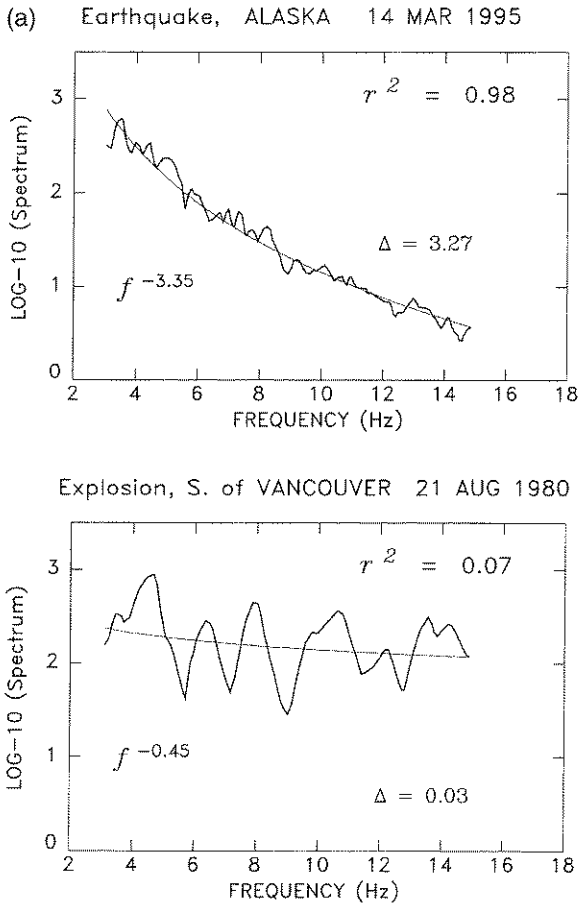

Figure 5. (a) Amplitude spectra of typical records of T phases from an earthquake (top) and an explosion (bottom), recorded by seismic stations deployed on atolls. Note that distances and maximum spectral amplitudes are comparable in both instances. The thick traces are the original spectral amplitudes, and the thin lines their best fit to a $f^{-\alpha}$ power law. The coefficient of correlation r^2 of ln $X(f)$ with ln f is given at the upper right. Note that the earthquake features a fast decaying, smooth spectrum (both α and r^2 large), but the explosion has a flat but irregular spectrum (both α and r^2 small). (b) Amplitude spectra for events I (left) and II (right) at WK31 (top) and PMO (bottom). Although the spectra feature some level of decay at the land station PMO, the best-fitting power α remains much lower than observed for earthquakes, and the discriminant Δ remains less than 1. Note that the spectra at the hydrophone station WK31 feature a poor correlation, suggestive of the influence of a bubble pulse.

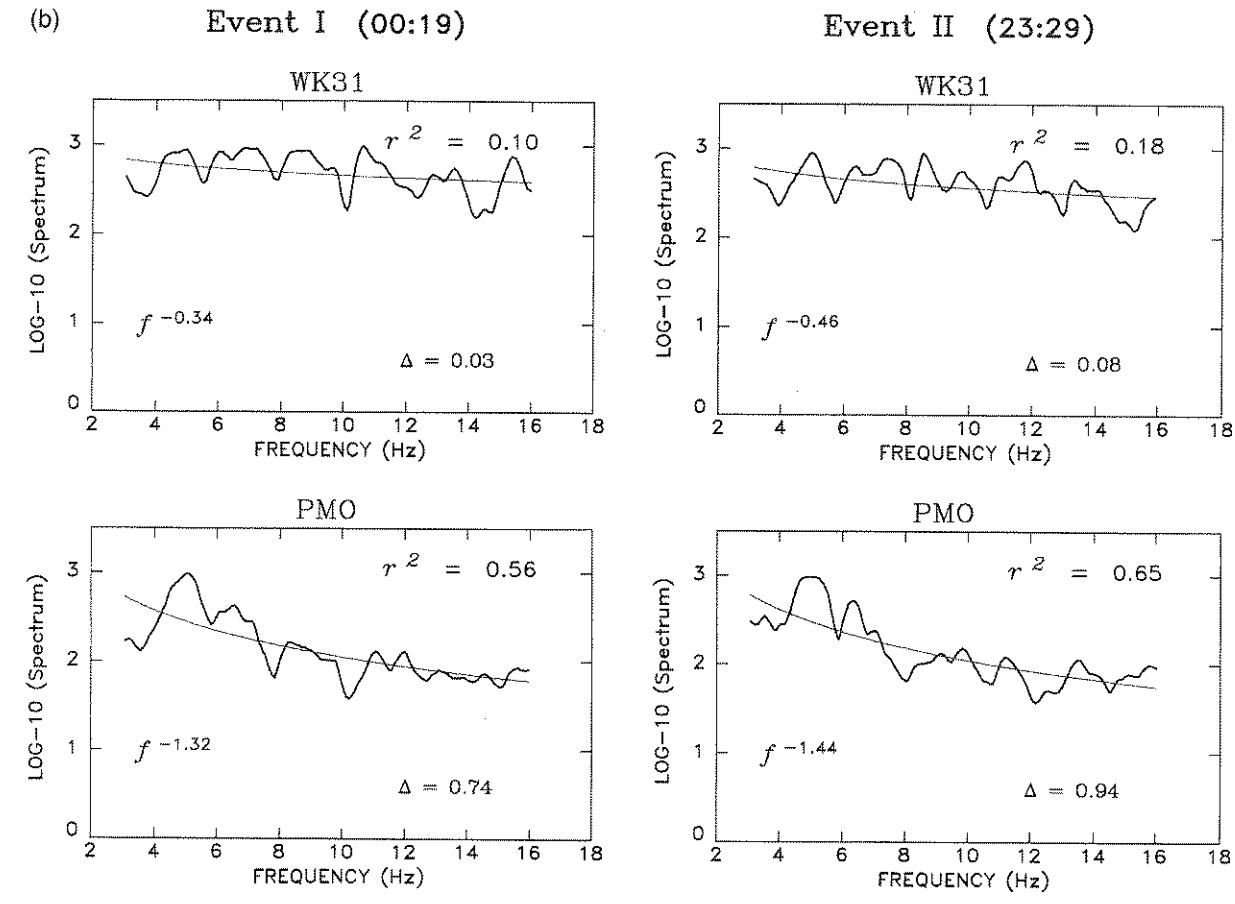

We quantify this behavior by fitting the amplitude $X(f)$ in the window 3–15 Hz with a power law of the form $f^{-\alpha}$, keeping track of the quality of the fit through the correlation coefficient r^2 between individual values of $\ln X(f)$ and $\ln f$. In the examples of Figure 5a, the regressed parameter α reaches 3.35 for the earthquake source, but remains low (0.45) for the explosion; conversely, the correlation coefficient r^2 is excellent (0.98) in the case of the dislocation but mediocre (0.07) for the explosion, whose spectrum is controlled by the bubble effect (Cole, 1948).

On the basis of our experience with a dataset of 206 records, of which Figure 5a presents typical examples, most explosions feature $\alpha < 1.4$, and most earthquakes have $\alpha > 1.5$. However, the discriminant α does not totally separate the populations, because a few records from explosions can occasionally feature α as large as 2.5, and earthquakes occurring in midplate volcanic structures, such as the flanks of Kilauea (the so-called "*H*" events described by Talandier and Okal [2001]), can have α as low as 1.2. Similarly, the correlation coefficient r^2 is generally smaller than 0.7 for most explosions, and greater than 0.75 for most earthquakes, with occasional exceptions: a few small Hawaiian earthquakes featuring r^2 as low as 0.57, and some explosions featuring a smooth spectrum with r^2 as large as 0.9, possibly as a result of firing procedures specially designed to eliminate the bubble "period" in seismic reflection experiments (Pascouët, 1991; Avedik *et al.*, 1993). Finally, we also consider the product of the two parameters,

$$\Delta = \alpha \cdot r^2 \tag{4}$$

to characterize the shape of the ground velocity spectrum; most earthquakes would feature $\Delta \geq 1.5$ and most explosions $\Delta \leq 1$, with a number of exceptions.

In very general terms, these observations can be explained, in the case of underwater explosions following Cole (1948), who modeled the pressure signal as a narrow pulse decaying exponentially with a decay time θ_s, growing with yield but always much shorter than the typical periods considered here. During the acoustic $\rightarrow$ seismic conversion at the receiver, the transmitted seismic velocities are expected to scale with the pressure of the incident oceanic wave, and thus the velocity spectrum of the recorded *T* phase should be the Fourier transform of an exponential pulse, essentially flat at frequencies much lower than $1/\theta_s$. In addition, for an underwater explosion, the spectrum will be perturbed by the so-called "bubble effect" resulting from the pulsation of the gas sphere comprising the products of the explosion (e.g., Cole, 1948; Hamilton and Patterson, 1965; Barrodale *et al.*, 1984; Chapman, 1985; Piserchia; 1998).

By contrast, in the case of an earthquake source, the *T* wave train recorded by a teleseismic atoll station is essentially a transcription of the strong ground motion at the source-side conversion point(s) (Talandier and Okal, 1998), the latter being multiple if the conversion takes place along a gentle slope (de Groot-Hedlin and Orcutt, 1999). At the frequencies characteristic of SOFAR propagation, the far-field displacement source spectrum should decay as f^{-3} for a simple seismic dislocation source (Haskell, 1966; Aki, 1967; Geller, 1976), or f^{-2} under the effect of additional complexities of the source process, such as stopping phases (Savage, 1974), the systematic presence of subsources (Blandford, 1975), and the thermal limitation of fault width on steeply dipping faults (Aki, 1972), a result also suggested by the dynamic model of Brune (1970, 1971). Evernden *et al.* (1986) have further suggested that the high-frequency source spectra of *P* and *S* waves, both of which are expected to contribute to the eventual *T* phase, may involve different power law coefficients α.

Depending on the exact contribution of such effects, we can reasonably expect $\alpha = 1.5$–3 for the velocity field at the source-side conversion point (as eventually recorded by a typical *T*-phase station). These values also reflect anelastic attenuation along the source-side seismic path, another source of depletion of high frequencies, obviously absent from an underwater explosion. The exception would be the *H* events, located in the immediate vicinity (at most a few kilometers) of a relatively steep, efficient conversion point, where the ground displacement could be controlled by the near-field terms, resulting in a drop of one unit for the parameter α (the effect of source-side seismic attenuation being also minimized for such events). Spectra decaying as f^{-2} have indeed been observed in the very near field by McGarr *et al.* (1990).

The contrast in values of α for the two kinds of sources can be regarded as due primarily to the difference in the order of magnitudes of the relevant corner frequencies, and such very crude models then justify the possibility of identifying the nature of a source of *T* phases from the variation of ground velocity spectral amplitude with frequency, with the remaining possible difficulty of the Hawaiian-type (*H*) earthquakes.

On Figure 5b, we apply this approach to the records of events I and II, at stations PMO and WK31. (We use seismic stations on atolls, and eliminate XMAS, where the 20-Hz sampling rate is too low. We consider neither WK30, whose instrument response is peaked at higher frequencies than at WK31, nor H25, whose frequency response is undocumented and where dynamic range is very low.) The power law coefficients obtained at PMO ($\alpha = 1.32$ and 1.44, respectively), as well as the correlation coefficients $r^2 = 0.56$ and 0.65, and the combined parameters $\Delta = 0.74$ and 0.94, are significantly lower than for earthquake sources, and support an explosive nature for the sources. (In the absence of any volcanic edifices in the epicentral area, we can rule out interpreting the events as volcanic, *H*-type earthquakes.) At WK31, we note the low values of the power law coefficients ($\alpha = 0.34$ and 0.46, respectively), but do not interpret them further, given the lack of a sufficient database of comparable records for hydrophone stations. We note, however, the strongly irregular character of the spectra ($r^2 = 0.10$ and 0.18, respectively).

Bubble Parameters

We proceed here with the formal analysis of the cepstra of the hydrophone records at WK30, WK31, and H25, which are essentially the inverse Fourier transform of the logarithm of their spectral amplitude (e.g., Kanasewich, 1981); the cepstrum features sharp peaks at the "quefrency" corresponding to the time offset of any (possibly damped) multiple phase or "echo" present in the time series. We restrict ourselves to the hydrophone records, sampled at 240 and 250 Hz, respectively. (The possible extension of the method to land-based stations is discussed in the Discussion and Conclusions section.) Our results (Fig. 6) show a consistent spike at quefrencies of 0.45 sec for event I, and 0.44 sec for event II.

The quefrency Q of the spike is the "period" of pulsation of the bubble generated by the explosion, and has been related to its depth h and yield Y, through the empirical formula proposed by Chapman (1985).

$$Q = 2.1 \frac{Y^{1/3}}{(h + 10.1)^{5/6}} \tag{5}$$

where Q is in seconds, Y in kilograms of equivalent TNT, and h in meters. In principle, the question of the trade-off between Y and h can be addressed through a comparison of amplitudes recorded on Polynesian atolls for the 2000 events and explosions with published source parameters (Nava *et al.*, 1988; Weigel, 1990; Talandier and Okal, 2001), taking into account an appropriate distance correction. We conclude that a possible scenario would involve a yield of 275 kg fired at a depth of 50 m, but these figures must remain tentative, given the trade-off between yield and depth in equation (5).

Frequency Dispersion of the Wavetrain

As mentioned under Data Processing and Source Location, T waves recorded at atoll stations from documented underwater explosive sources exhibit a clear inverse dispersion, which we have modeled using equation (1). On the other hand, on the basis of a dataset of more than 80 records, we fail to reproduce this observation in the case of earthquake sources, including H events occurring in intraplate "hotspot" environments. We illustrate this difference in behavior in the top frames of Figure 7, which contrast the undispersed wave train of a small Hawaiian earthquake (a) with the sharply dispersed T phase of a reported explosion off the Washington Coast (b), recorded at the same station (Tiputa, Rangiroa). As a result, and from an empirical standpoint, the presence of a strongly dispersed wave train can be used as an auxiliary and qualitative criterion of discrimination. We tentatively attribute this difference in dispersion properties to a difference in the excitation of the various modes composing the wave channeled into the SOFAR (Jensen *et al.*, 1994), the earthquake sources probably involving a higher number of modes (D'Spain *et al.*, 2001), relative to the simpler case of an explosive source (Heaney *et al.*, 1991).

Figure 7c shows event II, with a clear difference in arrival times of 1.0 sec between the two frequency bands considered, 4–5 Hz in red and 8–10 Hz in blue. This behavior supports the interpretation of the source of the wave train as an underwater explosion.

Discussion and Conclusions

A first conclusion of this study is that careful routine processing of seismic records at oceanic T-wave stations can extract and identify unannounced underwater explosions of relatively small yields at teleseismic distances. Although the accuracy of the epicenters reported here cannot be assessed without ground-truth information, the various tests performed in the Data Processing and Source Location section indicate a precision of ± 2 km, sufficient to separate the epicenters of events I and II.

In this respect, the availability of stations deployed on atoll structures, where the postconversion seismic path is minimized, is critical, as emphasized previously (Okal, 2001; Talandier and Okal, 2001). The performance of these stations is found to be crucial both at the detection, location, and interpretation stages.

On a related topic, we wish to comment here on our choice of station BNB, on the Queen Charlotte Islands, Canada, as opposed to the International Monitoring System (IMS) hydroacoustic station HA02, deployed at Van Inlet (VIB). In the Spring of 2000, BNB was being operated as part of an experimental network on the Queen Charlotte Islands, to test the variability of various recording parameters on a regional scale (McCormack and Woodgold, 2000). Because of the proximity of BNB to a segment of coastline where the continental shelf is narrow and the underwater slopes relatively steep, it is straightforward to calculate an adequate path correction $C = -2.05$ sec. By contrast, VIB is located along a segment of coast where an isobath typical of the SOFAR axis (1200 m) moves out at sea as much as 30 km, featuring a gently dipping slope and hence a complex acoustic $\rightarrow$ seismic conversion (de Groot-Hedlin and Orcutt, 2001). The geometry off VIB casts some doubt on the precise location and mechanism of the conversion, whose modeling would have been necessary to predict an adequate value of the correction C. We conclude that BNB is indeed a better site than VIB from the standpoint of locating T-phase epicenters.

A second lesson learned from the detection and investigation of events I and II is the excellent synergy that can be achieved between seismic and hydroacoustic stations. In particular, the precision of our locations was dramatically improved by including the three hydrophone stations; without them, the dataset loses resolution in the west-northwest–east-southeast direction, resulting in a displacement of the epicenter of event I of 4 km, and in an elongated Monte Carlo ellipse with a 5.7-km semimajor axis. Although this

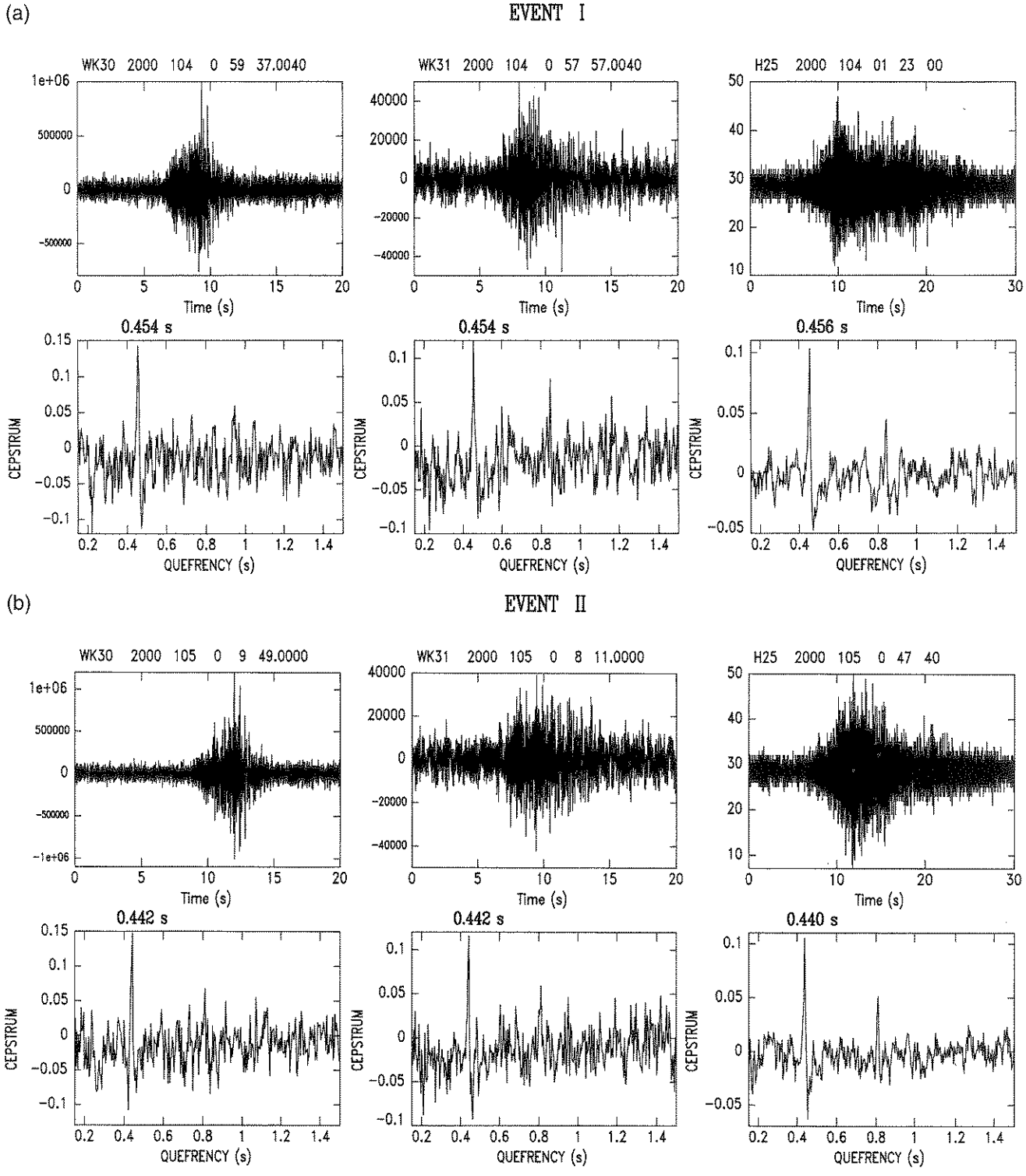

Figure 6. (a) Investigation of the bubble pulse in the records of event I at the hydrophone stations WK30, WK31, and H25. Top, Individual time series; the vertical scales are arbitrary digital units. Bottom, Cepstrum of the windowed time series at each location. Note the consistent spike at the quefrency 0.455 ($\pm$0.001) sec. The second maximum in the cepstrum, at about 0.82 sec, emerges marginally from the background noise at WK31 and H25. (b) Same as Figure 6a for event II.

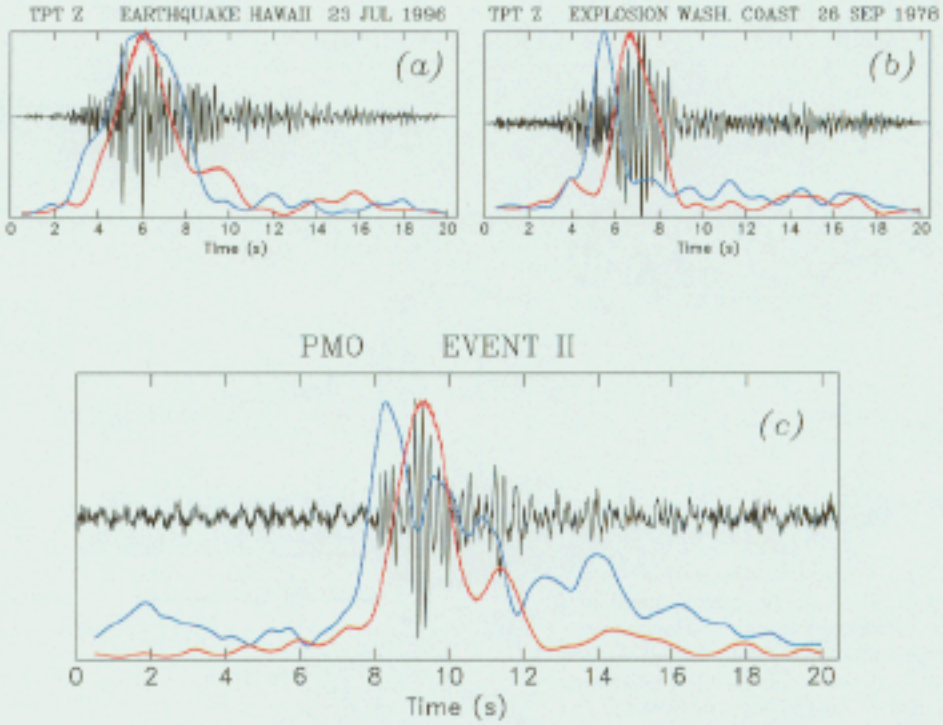

Figure 7. Investigation of the frequency dispersion of the waveform. In each frame, the black trace is the T wave train, high-pass filtered at 2 Hz; the red trace is the envelope of the signal band-pass filtered between 4 and 5 Hz; the blue one the envelope between 8 and 10 Hz. The top frames show typical waveforms recorded at TPT (Tiputa, Rangiroa) from a Hawaiian earthquake (a) and a documented explosion off the coast of Washington (b). Note that the latter exhibits a clear separation between the two envelopes, illustrating a strong frequency dispersion during the propagation, which is absent in the former. The bottom frame (c) shows the case of event II recorded at PMO, illustrating a clear frequency dispersion.

particular geometry obviously reflects the lack of adequate seismic records to the east and west of the sources, our results stress the value of combining datasets involving different technologies.

Regarding a possible direct comparison of the size of the events, Figure 8 explores the ratio of the spectral amplitudes $X(f)$ recorded for events I and II at the three stations WK31 (hydrophone), PMO (seismic, atoll), and KAA (seismic, steep basalt flow). The simplest ratio is obtained at WK31 where the two signals differ less than 0.1 logarithmic unit at frequencies below 10 Hz, with the two sources best described as equivalent. At KAA, in contrast, we observe a decreasing trend of $X_{II}(f)/X_I(f)$ with increasing f, with a minimum of -0.2 logarithmic units (a factor of 0.6) reached at ~9 Hz. A similar trend is observed at PMO, but the minimum is reached at a lower frequency (6 Hz), and the spectrum of event II is consistently greater (by an average of 0.15 logarithmic units or a factor of 1.4) than that of event I. We conclude that the detailed spectrum of T waves sent in different azimuths from what must have been, under all probability, two very similar sources (we recall that the bubble periods are essentially indistinguishable), must be sensitive to minute details in the exact location, depth, yield, and possibly firing process, which cannot be speculated on further in the absence of ground truth information.

With regard to source discrimination, we have tested the feasibility of using the duration–amplitude discriminant D introduced by Talandier and Okal (2001), emphasizing its preferential performance at seismic stations located on atolls, and generalizing its use outside Polynesia. We also find that other, more empirical, potential discriminants, such as the power law exponent α and the correlation coefficient r^2 may serve in a complementary fashion to verify the nature of the source, while stressing that significant differences may exist between seismic and acoustic records. The presence of a clear inverse dispersion of group arrival times with frequency can also serve as a complementary discriminant.

The bubble effect is well observed in hydrophone records and at some land-based sites, and it can be quantified by cepstral analysis to retrieve the so-called "bubble period" related to the depth and yield characteristics of the sources. However, in all applications involving detailed investigation of frequency spectra, a crucial parameter is the sampling rate of the relevant time series, which controls the Nyquist fre-

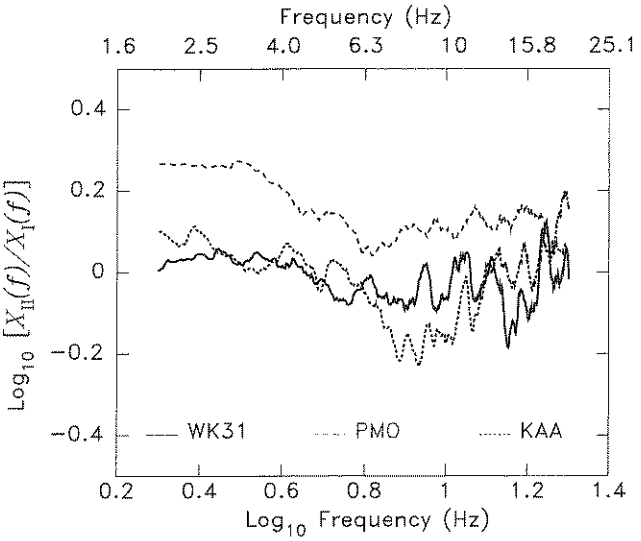

Figure 8. Variation as a function of frequency f of the ratios $X_{II}(f)/X_I(f)$ of the spectral amplitudes recorded at the hydrophone station WK31 (solid line), the atoll seismic station PMO (long dashes) and the station KAA (short dashes), deployed along the steep basaltic cliffs of the island of Hawaii. Note the disparity in behavior of the ratio at the three sites.

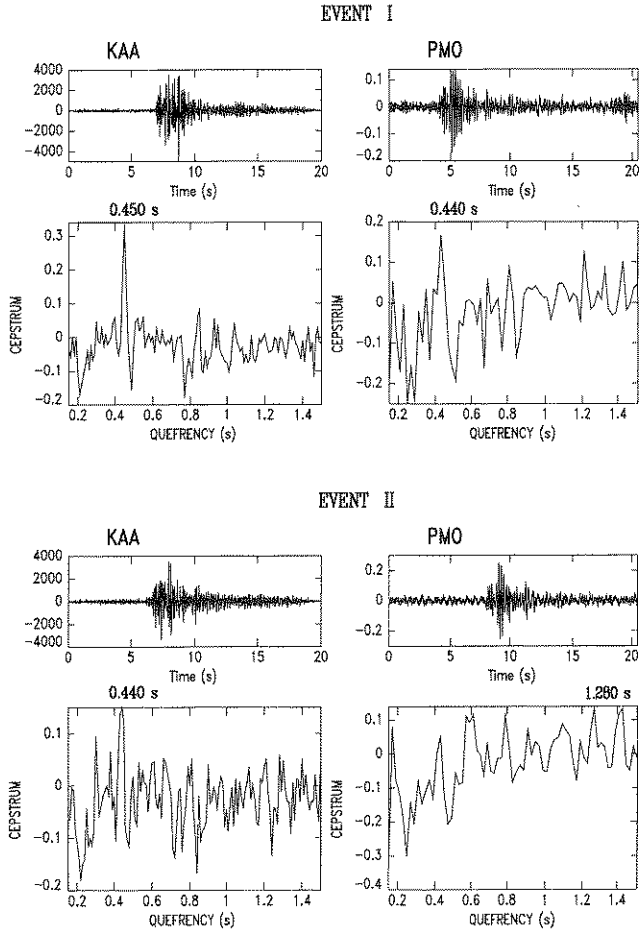

Figure 9. Extension of cepstral investigation to land-based stations KAA (left) and PMO (right). Note the generally lower signal-to-noise ratios at PMO. The bubble spike in the cepstrum is well extracted only for event I at KAA.

quency. We illustrate this limitation on Figure 9, which presents the cepstra of the land-based records at KAA and PMO, the former using a sampling rate of 100 Hz, the latter 50 Hz. At KAA, the spike of event I is extracted at a quefrency of 0.45 sec, in full agreement with the hydrophone results; at PMO, the maximum of the cepstrum is indeed found at Q = 0.44 sec, but the sampling is too coarse to give it the character of an undisputed spike. In event II, the spike is tentatively identified in the KAA cepstrum, but does not emerge from background noise at PMO. We conclude that, although land-based T-phase stations have the potential to resolve bubble periods, a high sampling rate, on the order of 100 Hz, is an absolute necessity. In this respect, the traditional sampling rate of 20 Hz used in the broadband IRIS stations was found to be insufficient to allow an adequate study of the decay parameter α, let alone to resolve the bubble periods. Even the improved sampling of 40 Hz, now available at many IRIS sites, may be too coarse for the latter.

A disappointing aspect of our investigation remains the large number of oceanic seismic stations that could not provide usable data, and this warrants some discussion. As documented in Table 1, one RSP station and no fewer than four IRIS stations on Pacific islands were not operating in the Spring of 2000. (In addition, KIP went down between the two events.) This is particularly unfortunate because RAR, for example, is a choice site for recording T phases (Adams, 1979; Okal and Talandier, 1997; Okal *et al.*, 2002). In addition, four Pacific island sites (KWAJ, PTCN, WAKE, and RPN), although operating, provided no detectable signal above ambient noise level. We verified that WAKE (but not the hydrophone sites WK30 and WK31) is blocked at the relevant backazimuth by a nearby seamount. As for Pitcairn (PTCN), the small size (4.5 km^2) of the young volcanic island renders the site noisy. An explanation for the absence of signal at RPN may be sought in its location at the center of the large unreefed Easter Island edifice, a gently sloping shield volcano, in a geometry unfavorable to acoustic–seismic conversion (Talandier and Okal, 1998), indeed, T-wave reception at RPN has been shown to be erratic (Okal and Talandier, 1997; Okal *et al.*, 2003), and a systematic study of the conditions of recording of T phases at RPN may be warranted. Finally, KWAJ is located on the southwestern side of Kwajalein Atoll, causing a 25-km-long postconversion land path, sufficient to attenuate the signal below noise level. These remarks reaffirm, if need be, the prime importance of an optimal location of the sensor in the installation of a high-performance T-phase station. In particular, in a large atoll such as Kwajalein, the instrumentation of the site with several sensors would provide much improved detection capa-

bilities. This strategy, which consists of operating an array of several stations to achieve full backazimuthal coverage, was applied at RSP (Okal *et al.*, 1980), and was also made part of the standard configuration of hydrophone stations of the IMS (Lawrence *et al.*, 2000).

Acknowledgments

In addition to the staff of the data centers at IRIS and PIDC, we are grateful to the following colleagues, who kindly provided data from their institutions allowing a broad geographic coverage: Alison Bird (Canadian National Seismic Network); Paul Okubo (Hawaii Volcano Observatory); Robert Cessaro (Pacific Tsunami Warning Center); and Robert Dziak (Hatfield Marine Science Center). Brian Lewis provided ground truth for the 1978 shots used to derive equation (1). We thank Seth Stein for discussion. Associate Editor Anton Dainty and two anonymous reviewers provided useful comments on the original version of the paper. This research was supported by the Defense Threat Reduction Agency of the Department of Defense under Contract DTRA01-00-C-0065. Maps were drawn using the GMT software (Wessel and Smith, 1991).

References

Adams, R. D. (1979). *T*-phase recordings at Rarotonga from underground nuclear explosions, *Geophys. J. R. Astr. Soc.* **58,** 361–369.

Aki, K. (1967). Scaling law of seismic spectrum, *J. Geophys. Res.* **72,** 1217–1231.

Aki, K. (1972). Scaling law of earthquake time-function, *Geophys. J. R. Astr. Soc.* **31,** 3–25.

Avedik, F., V. Renard, J.-P. Allenou, and B. Morvan (1993). "Single bubble" air-gun array for deep exploration, *Geophysics*, **58,** 366–382.

Barrodale, I., N. R. Chapman, and C. A. Zala (1984). Estimation of bubble pulse wavelets for deconvolution of marine seismograms, *Geophys. J. R. Astr. Soc.* **77,** 331–341.

Blandford, R. R. (1975). A source theory for complex earthquakes, *Bull. Seism. Soc. Am.* **65,** 1385–1405.

Brune, J. N. (1970). Tectonic stress and the spectra of seismic shear waves from earthquakes, *J. Geophys. Res.* **75,** 4997–5009.

Brune, J. N. (1971). Correction, *J. Geophys. Res.* **76,** 5002.

Chapman, N. R. (1985). Measurement of waveform parameters of shallow explosive charges, *J. Acoust. Soc. Am.* **78,** 672–681.

Cole, R. H. (1948). *Underwater Explosions*, Princeton Univ. Press, Princeton, New Jersey, 437 pp.

D'Spain, G. L., L. P. Berger, W. A. Kuperman, J. L. Stevens, and G. E, Baker (2001). Normal mode composition of earthquake *T* phases, *Pure Appl. Geophys.* **158,** 475–512.

de Groot-Hedlin, C. D., and J. A. Orcutt (1999). Synthesis of earthquake-generated *T* waves, *Geophys. Res. Lett.* **26,** 1227–1230.

de Groot-Hedlin, C. D., and J. A. Orcutt (2001). *T*-phase observations in Northern California: Acoustic to seismic coupling at a weakly elastic boundary, *Pure Appl. Geophys.* **158,** 513–530.

Evernden, J. F., C. B. Archambeau, and E. Cranswick (1986). An evaluation of seismic decoupling and underground nuclear test monitoring using high-frequency seismic data, *Rev. Geophys.* **24,** 143–215.

Fox, C. G., H. Matsumoto, and T.-K. Lau (2001). Monitoring Pacific Ocean seismicity from an autonomous hydrophone array, *J. Geophys. Res.* **106,** 4183–4206.

Geller, R. J. (1976). Scaling relations for earthquake sources and magnitudes, *Bull. Seism. Soc. Am.* **66,** 1501–1523.

Hamilton, G., and B. Patterson (1965). Spectra of large underwater explosions, *J. Acoust. Soc. Am.* **38,** 941 (A).

Haskell, N. A. (1966). Total energy and energy spectral density of elastic wave radiation from propagating faults, *Bull. Seism. Soc. Am.* **56,** 125–140.

Heaney, K. D., W. A. Kuperman, and B. E. McDonald (1991). Perth-Bermuda sound propagation (1960), *J. Acoust. Soc. Am.* **90,** 2586–2594.

Jensen, F. B., W. A. Kuperman, M. B. Porter, and H. Schmid (1994). *Computational Ocean Acoustics*, Am. Inst. Phys. Press, New York, 612 pp.

Kanasewich, E. R. (1981). *Time Sequence Analysis in Geophysics*, Univ. Alberta Press, Edmonton, 480 pp.

Lawrence, M., M. Galindo, P. Grenard, and J. Newton (2000). The hydroacoustic network, International Monitoring System: Status and plans, in *Proc. 22nd Seism. Res. Symp.*, New Orleans, Louisiana, 12–15 September 2000, U.S. Dept. of Defense, vol. III, pp. 51–54 (abstract).

Levitus, S., T. P. Boyer, J. Antonov, R. Burgett, and M. E. Conkright (1994). *World Ocean Atlas 1994*, NOAA/NESDIS, Silver Spring, Maryland.

McCormack, D. C., and C. Woodgold (2000). *T*-phase observations at HA02 and the design of *T*-phase stations for the IMS, in *Proc. Informal Workshop on Hydroacoustics*, Papeete, 27 September–1 October 1999, Commiss. Energie Atomique, Paris, pp. 241–259 (abstract).

McGarr, A., J. Bicknell, J. Churcher, and S. Spottiswoode (1990). Comparison of ground motion from tremors and explosions in deep gold mines, *J. Geophys. Res.* **95,** 21,777–21,792.

Nava, F. A., F. Núñez-Cornu, D. Córdoba, M. Mena, J. Ansorge, M. Rodríguez, E. Banda, S. Müller, A. Udías, M. García-Garca, G. Calderón, and the Mexican Working Group for Deep Seismic Profiling, Structure of the Middle America Trench in Oaxaca, Mexico (1988). *Tectonophysics* **154,** 241–251.

Okal, E. A. (2001). *T*-phase stations for the International Monitoring System of the Comprehensive Nuclear-Test Ban Treaty: A global perspective, *Seismol. Res. Lett.* **72,** 186–196.

Okal, E. A., and J. Talandier (1997). *T* waves from the great 1994 Bolivian deep earthquake in relation to channeling of *S* wave energy up the slab, *J. Geophys. Res.* **102,** 27,421–27,437.

Okal, E. A., P.-J. Alasset, O. Hyvernaud, and F. Schindelé (2003). The deficient *T* waves of tsunami earthquakes, *Geophys. J. Int.* **152,** 416–432.

Okal, E. A., J. Talandier, K. A. Sverdrup, and T. H. Jordan (1980). Seismicity and tectonic stress in the southcentral Pacific, *J. Geophys. Res.* **85,** 6479–6495.

Pascouët, A. P. (1991). Something new under the water: the bubbleless air gun, *Leading Edge* **10,** no. 11, 79–81.

Piserchia, P.-F. (1998). Propagation et conversion des ondes *T* par simulation numérique hybride, Thèse de Doctorat, Univ. Nice Sophia-Antipolis.

Savage, J. C. (1974). Relation between *P*- and *S*-wave corner frequencies in the seismic spectrum, *Bull. Seism. Soc. Am.* **64,** 1621–1627.

Taber, J. J., and B. T. R. Lewis (1986). Crustal structure of the Washington continental margin from refraction data, *Bull. Seism. Soc. Am.* **76,** 1011–1024.

Talandier, J., and G. T Kuster (1976). Seismicity and submarine volcanic activity in French Polynesia, *J. Geophys. Res.* **81,** 936–948.

Talandier, J., and E. A. Okal (1998). On the mechanism of conversion of seismic waves to and from *T* waves in the vicinity of island shores, *Bull. Seism. Soc. Am.* **88,** 621–632.

Talandier, J., and E. A. Okal (2001). Identification criteria for sources of *T* waves recorded in French Polynesia, *Pure Appl. Geophys.* **158,** 567–603.

Thomson, D. J., and A. D. Chave (1991). Jacknifed error estimates for spectra, coherences, and transfer functions, in *Advances in Spectrum Analysis and Array Processing*, S. Haykin (Editor), Vol. 1, Prentice Hall, New York, 58–113.

Weigel, W. (1990). *Bericht über die SONNE-Expedition SO65-2, Papeete–Papeete, 7.–28. Dez. 1989,* Universität Hamburg, Institut für Geophysik.

Wessel, P., and W. H. F. Smith (1991). Free software helps map and display data, EOS **72,** 441 and 445–446.

Wysession, M. E., E. A. Okal, and K. L. Miller (1991). Intraplate seismicity of the Pacific Basin, 1913–1988, *Pure Appl. Geophys.* **135,** 261–359.

Laboratoire de Géophysique
Commissariat à l'Energie Atomique
Boîte Postale 640
F-98713 Papeete, Tahiti, French Polynesia
(D.R., O.H.)

Département Analyse et Surveillance de l'Environnement
Commissariat à l'Energie Atomique
Boîte Postale 12
F-91680 Bruyères-le-Châtel, France
(J.T.)

Department of Geological Sciences
Northwestern University
Evanston, Illinois 60208
(E.A.O.)

Manuscript received 30 November 2001.